Int J Adv Manuf Technol (2016) 85:1347–1360
DOI 10.1007/s00170-015-8019-9

ORIGINAL ARTICLE

A water dissolution method for removing micro-waviness caused by SPDT process on KDP crystals

Xu Wang[1] · **Hang Gao**[1] · **Yuchuan Chen**[1] · **Dongming Guo**[1]

Received: 8 June 2015 / Accepted: 25 October 2015 / Published online: 6 November 2015

Abstract Single crystals of potassium dihydrogen phosphate (KDP) are an irreplaceable optical material in laser-induced inertial confinement fusion (ICF), where they are used as electro-optic switches and for laser-frequency conversion. The KDP lenses used in ICF applications must be pristine, high quality, and have a surface roughness of less than 3 nm. Currently, single-point diamond turning (SPDT) is the primary method for performing ultra-precision machining on KDP crystals. However, after the SPDT process, the crystal surface exhibits micro-waviness and subsurface damage, both of which have adverse effects on the optical performance of the KDP elements, especially the laser-induced damage threshold. In this study, a new method of micro-dissolution polishing was developed, which is based on the solubility of KDP crystals in water, to achieve controllable material removal. A material removal function was formulated to describe the material removal in terms of both the path and parameters used to polish the SPDT-machined samples with a small polishing tool. An experimental study showed that this method is able to reduce the surface micro-waviness and surface roughness (from 6.205 to 2.107 nm) significantly. The method is also applicable to the polishing of other water-soluble materials.

Keywords KDP single crystals · Micro-waviness · Water dissolution · Material removal · Surface roughness

✉ Hang Gao
hanggao4187@126.com

[1] Key Laboratory for Precision and Non-traditional Machining Technology of Ministry of Education, Dalian University of Technology, Dalian 116024, People's Republic of China

1 Introduction

Single crystals of potassium dihydrogen phosphate (KDP) possess excellent non-linear electro-optical properties and are currently the only material suitable for electro-optic switches and laser-frequency conversion applications in laser-induced inertial confinement fusion (ICF) [1]. ICF requires a large number of high-quality KDP elements with large apertures (0.5–1 m) every year. For example, the American National Ignition Facility (NIF) has 192 identical beam lines that use 550 KDP lenses [2]. In 2013, the NIF made a significant breakthrough by creating a greater output energy than the input energy for the first time [3]. It is predicted that the demand for high-quality KDP elements will increase with the progression of ICF technology.

KDP crystals are difficult to machine because of their inherent softness, brittleness, and deliquescence, as well as their strong anisotropy and temperature sensitivity. Thus, it is extremely hard to obtain KDP elements that meet the requirements of ICF applications (root mean square (rms) surface roughness ≤5 nm; transmission wavefront distortion ≤λ/6 peak-to-valley (PV); laser-induced damage threshold ≥15 J/cm^2).

A variety of ultra-precision machining techniques has been investigated for the processing of KDP crystals. Yoshiharu et al. [4] obtained a super-smooth KDP sample with a rms surface roughness of 0.553 nm via ultra-precision grinding. Peng et al. [5] and Arrasmith et al. [6] processed KDP crystals via magnetorheological finishing (MRF) and achieved satisfactory results (surface roughness of approximately 2 nm). Wang et al. [7] polished KDP samples with the traditional polishing method. SiO_2 powders with particle diameters of 7–20 nm were used as the abrasive in the polishing process, and a super-smooth surface with a surface roughness 2–3 nm was obtained. However, abrasive particles were embedded in

the surface of the samples and scratches would randomly appear on the polished surfaces.

Single-point diamond turning (SPDT) is currently the most important ultra-precision machining method for KDP crystals [8], and the elements machined with this technique possess a low roughness and high surface figure [9]. However, during the SPDT process, a KDP workpiece is fed along the radial direction of the rotational motion of the diamond tool (Fig. 1). The feeding pitch causes the formation of cutting marks (micro-waviness), which adversely affect the optical performance of the KDP element, especially the laser-induced damage threshold [10]. To minimize the degree of micro-waviness and improve the quality of KDP lenses, many studies have focused on designing and optimizing machine tools for the machining of large KDP crystals [11, 12].

In general, subsurface damage is inescapable when using a process that mechanically removes material from a workpiece. The depth of the subsurface damage caused by SPDT varies from dozens of nanometers to several micrometers, depending on the cutting parameters [13]. The damaged subsurface layer can adversely affect the optical properties of KDP lenses. Figure 2 shows that the micro-waviness is very difficult to remove because of its small scale (an amplitude of only dozens of nanometers). The problem of eliminating the micro-waviness without introducing any new damage to sample is an urgent issue that must be solved. Several methods have been attempted to remove the micro-waviness after SPDT processing. Jacobs [14] machined KDP crystals with the MRF method and found that an rms surface roughness of 2 nm could be achieved without any diamond-turning marks. Menapace et al. [15] removed micro-waviness via MRF and successfully improved the laser-induced damage threshold.

However, because subsurface damage is commonly caused by the mechanical removal of material, a damage-free machining method is required to improve the laser-induced damage threshold of KDP elements. For example, no mechanical stress is induced during the dissolution of a KDP crystal in water. Based on the solubility of KDP crystals in water, researchers have attempted to incorporate water into the machining of KDP crystals to decrease the degree of subsurface damage. Zhang et al. [16] polished KDP samples by exposing them to a mixed solution of water and alcohol. However, this treatment introduced a new problem in that alcohol absorbs water from the atmosphere, while the volatile nature of alcohol was not mentioned. Menapace et al. [15] added water to the MR fluid to eliminate KDP removed from the sample via precipitation and re-crystallization.

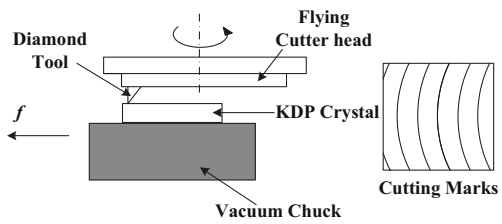

Fig. 1 Schematic diagram of a SPDT setup

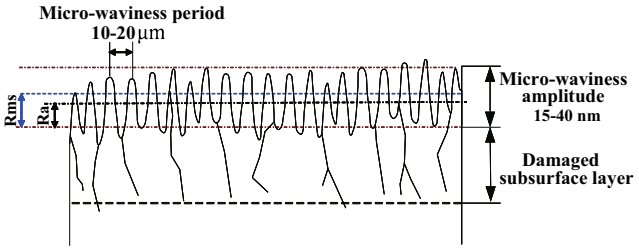

Fig. 2 Schematic diagram showing the micro-waviness of a SPDT-treated KDP surface

Recently, the authors of this study have performed much research on developing KDP machining technology that is based on the water-soluble nature of KDP. Wang et al. [17] invented a type of water-in-oil (W/O) micro-emulsion fluid that can be used as an abrasive-free polishing fluid. The characteristics (e.g., conductivity, viscosity, diffusion coefficient, and droplet size) of this fluid were investigated, and the existence of the W/O structure was confirmed. The feasibility of using such a W/O micro-emulsion fluid to machine KDP crystals was demonstrated with small KDP samples.

The objective of this study was to process KDP crystals with water to achieve a low-stress machining technique and remove the deficiencies introduced by common machining methods. A new method for polishing KDP with a W/O polishing fluid was developed to achieve this objective. By using the solubility of KDP in water during the machining process, a nearly damage-free super-smooth surface was obtained. In terms of a material removal function [18], a computer-controlled micro-dissolution polishing method for KDP was developed by combining it with a computer-controlled optical-surfacing technique and a planned polishing path. A small tool was used to polish the KDP samples after the initial SPDT processing. The feasibility of removing the micro-waviness of large-aperture KDP crystals with the novel method developed in this study is also discussed in this paper.

2 Computer-controlled micro-dissolution polishing method

2.1 Principles of micro-dissolution polishing

The solubility of a KDP crystal in water is 33 g per 100 g of water at 25 °C. If exposed to the atmosphere, an ultra-precision-machined KDP surface can be destroyed by the water absorbed from the air. Therefore, because of the high water solubility, there are extra challenges when machining and storing KDP crystals.

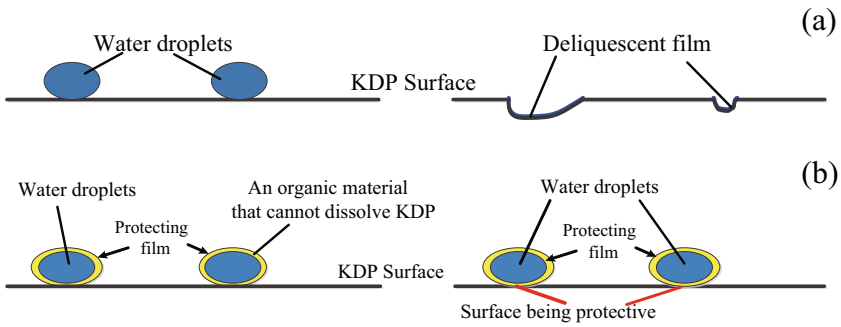

Fig. 3 Schematic diagram showing the effects of water droplets that are **a** directly touching the surface of a KDP crystal and **b** wrapped in a protective film. The water droplets wrapped in a protective film cannot dissolve KDP

When a KDP crystal encounters water droplets, its surface is destroyed by the formation of dissolution pits (Fig. 3a). Conversely, if a microscale water droplet is enclosed in a protective organic film that does not dissolve the KDP crystal, the water droplet cannot directly touch the crystal; thus, the KDP surface is protected from dissolution by the organic film (Fig. 3b).

Based on the dissolution properties of a KDP crystal, a W/O-structured micro-emulsion was developed for use as a polishing fluid. Figure 4 shows a schematic diagram of micro-scale water droplets that are wrapped in a non-ionic surfactant, where one end is a hydrophilic group and the other end is hydrophobic group, and form water micelles in an oil-based solvent.

Figure 5 shows a schematic diagram of the selective removal of material via the micro-dissolution polishing method. During this polishing process, a small polishing tool moves along pre-defined paths. Outside of the polishing region, the W/O structure is maintained without any relative movement between the crystal and polishing pad; thus, the water micelles are dispersed in the organic solvent that neither dissolve nor react with the KDP surface, respectively. Therefore, the KDP surface is protected by the organic solvent from coming into direct contact with the water droplets, which are trapped in micro-micelles.

In the polishing area, at the points of contact between the polishing pad and KDP crystal, the water micelles are deformed by the shear force applied between the polishing pad and KDP crystal, and the water droplets are released and are able to dissolve the asperities of the KDP crystal. The dissolution layer is then removed by the mechanical friction of the polishing pad and the flow of the polishing fluid. Meanwhile, in the valleys of the KDP surface where the polishing pad does not directly contact the KDP crystal, the water micelles are stable and no dissolution should occur. Thus, the selective removal of material is achieved by ensuring micro-dissolution only occurs at the asperities of the crystal surface.

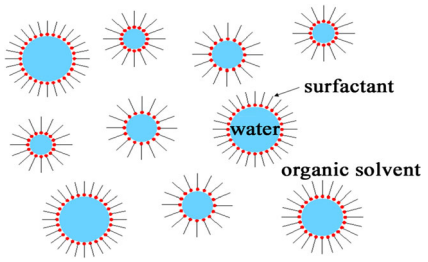

Fig. 4 Schematic diagram of a W/O-structured polishing fluid [19]

The size of the water micelles in the polishing fluid was measured via dynamic light scattering (DLS). Figure 6 shows that the dimensions of the water micelles are approaching a normal distribution. The diameters of the water micelles range from 1 to 10 nm, and the mean diameter is 1.4 nm.

In practical machining processes, a uniformly flat surface cannot be achieved. Even when the surface roughness was approximately 1 nm, there were still height differences of approximately 10–20 nm in the area measured (0.35 × 0.26 mm). In this case, the polishing fluid can improve the surface quality via the aforementioned technique. Thus, the properties required for the applications of KDP crystal can be satisfied.

However, there is still a minimum surface roughness that cannot be decreased further as the surface approaches a uniform flatness. Once this level of surface roughness is reached, the water micelles twist and break randomly under the shear force of the polishing pad in machining area, and an equilibrium is reached between the random dissolution and selective removal of material. On the macroscopic scale, this appears as the uniform removal of material, and the surface quality will not decrease after reaching the aforementioned limit.

To improve the limitations of this micro-dissolution polishing technique and reduce the surface roughness further, research should be conducted on methods to minimize the diameters of the water micelles in the polishing fluid. The results of such research may be reported in a future paper.

X-ray photoelectron spectroscopy (XPS, VG ESCALAB MK2) was used to determine the composition of a KDP sample before and after the polishing process with the W/O fluid, which was performed in the previous study by the authors' group [20]. The excitation source was Al-Kα ($h\nu$ = 1486.6 eV), while the working voltage and pressure were 12.5 kV and 3.5×10^{-6} Pa, respectively. The C, K, P, and O XPS spectra of the KDP crystal before and after the polishing

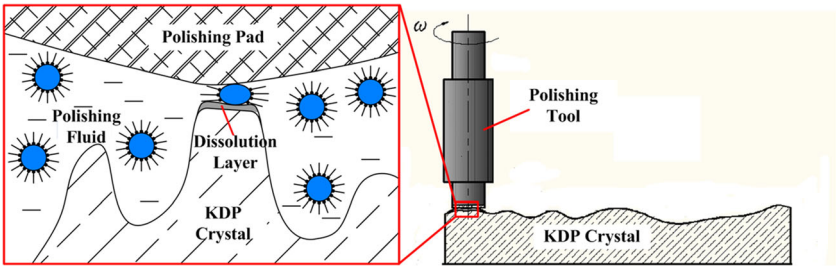

Fig. 5 Schematic diagram of the selective removal of material from a KDP crystal

are presented in Fig. 7. The spectra show that the characteristic peaks of the KDP crystal polished with the W/O fluid are identical to that of the KDP before polishing (KH_2PO_4). The absence of any new characteristic peaks indicates that no new compounds are produced during the polishing process, and after polishing, the surface is still a pure KDP crystal.

Computer-controlled optical surfacing techniques are widely used in the field of large-aperture optical surfacing, which involves the use of a small polishing tool to process optical elements [21, 22]. By incorporating the micro-dissolution mechanism into a computer-controlled optical surfacing technique, this study has developed a new method for KDP crystal polishing that uses a small polishing tool. In this method, the surface of the KDP crystal to be polished is divided into a grid, the amount of material removed from each grid point is determined by measuring the surface-figure error of the crystal, and then, an appropriate removal function is chosen to calculate the dwell time of the polishing tool at each grid point.

2.2 Formulating the material removal function

The Preston equation is widely employed in chemical-mechanical polishing (CMP) to describe the correlation between the material removal rate and polishing parameters. In this equation, the material removal rate is proportional to the polishing velocity (v) and polishing load (P), i.e., the polishing material removal rate, MRR$=KPv$, where K is the Preston coefficient.

However, in addition to v and P, MMR is also dependent upon the water content and temperature of the polishing fluid, the polishing pad material, and other factors during the micro-dissolution polishing of a KDP crystal. These factors are accounted for with K. During the polishing process, the polishing head executes a planetary motion, as shown in Fig. 8, and the polishing velocity at an arbitrary point, $P(r, \theta)$, can be determined according to Fig. 8. The MMR equation is shown in Eq. (1):

$$\mathrm{MRR}(r,\ \theta) = KP \int_{\alpha_1}^{\alpha_2} \sqrt{(n_{\mathrm{rot}} \pm n_{\mathrm{rev}})^2 e^2 + (n_{\mathrm{rot}} r)^2 - 2(n_{\mathrm{rot}} \pm n_{\mathrm{rev}}) n_{\mathrm{rot}} e r \cos(\theta - \alpha)}\, \mathrm{d}\alpha \tag{1}$$

where n_{rot} and n_{rev} are the rotational and revolving speeds of the polishing head, respectively; e is the eccentricity (radius of revolution); $a_1=\theta-\cos^{-1}[(e^2+r^2-r_0^2)/(2er)]$; and $a_2=\theta+\cos^{-1}[(e^2+r^2-r_0^2)/(2er)]$. When the directions of rotation and revolution are the same, the "±" in Eq. (1) becomes "+"; otherwise, it becomes "–."

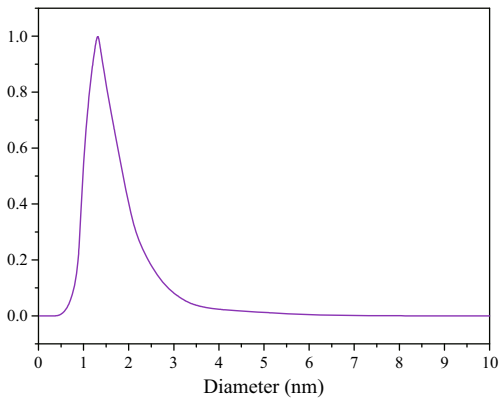

Fig. 6 Particle size distribution of the radii of the water micelles in the polishing fluid, as measured by DLS [20]

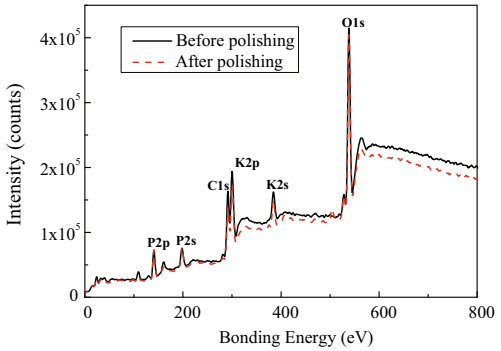

Fig. 7 XPS spectra of a KDP crystal before and after the polishing process [20]

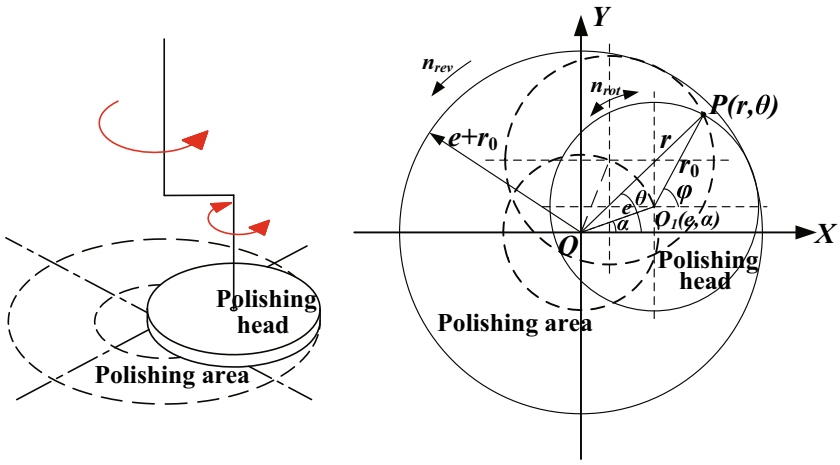

Fig. 8 The rotational and revolving motions of the polishing head

2.3 Polishing dwell time

After determining the correct MRR expression, a dwell-time distribution map (i.e., the time function for the polishing tool dwelling on each point of the crystal surface) is obtained. The dwell-point grid of the crystal surface is generated, and the initial surface-figure error is measured with an interferometer to determine the ideal amount of material to be removed at each dwell point (Fig. 9).

The polishing head moves along a pre-defined tool path during the polishing process, as shown in Fig. 10. The material removal equation for an arbitrary point is shown in Eq. (2):

$$E_{\mathrm{Final}}(x,\ y) = H_{\mathrm{Initial}}(x,\ y) - \mathrm{MRR}(x,\ y)\cdot D(x,\ y) \tag{2}$$

where $E_{\mathrm{Final}}(x,y)$ is the residual error distribution function of the surface after the polishing process, $H_{\mathrm{Initial}}(x, y)$ is the function describing the ideal amount of material to be removed (initial surface-figure error distribution map), and $D(x, y)$ is the dwell-time function.

During an ideal polishing process, the residual error is expected to be zero, i.e., $E_{\mathrm{Final}}(x, y)=0$. Thus, Eq. (2) can be transformed into Eq. (3).

$$D(x,\ y) = \frac{H_{\mathrm{Initial}}(x,\ y)}{\mathrm{MRR}(x,\ y)} \tag{3}$$

Figure 10 shows that the central revolving axis of the polishing head moves along a raster path. However, the polishing head cannot completely move to the edges of the crystal surface because of the eccentricity of the revolution; otherwise, it will result in the tilting of the polishing head. Therefore, a certain distance (D) is reserved between the starting point of the polishing path and edges of the crystal surface to avoid the tilting of the polishing head.

At $R(x, y)$ of the polishing path, the polishing head executes planetary motion around $R(x, y)$ with a dwell time of T_{xy}. $P_{xy}(r, \theta)$ represents the coordinates of an arbitrary point (P_{xy}) on the crystal surface where the material removal rate is given by $\mathrm{MRR}_{xy}(r, \theta)$. Therefore, the amount of material removed (H) at P_{xy} is given by Eq. (4):

$$H = \iint \mathrm{MRR}_{xy}(r,\ \theta) T_{xy}\,\mathrm{d}x\mathrm{d}y \tag{4}$$

which can be set to $H_{\mathrm{Initial}}(x, y)$. Thus, the discrete form of Eq. (4) is obtained (Eq. (5)):

$$\sum_{i=1,j=1}^{i=n,j=m} \mathrm{MRR}_{x_i y_j}(r_i,\ \theta_j) T_{x_i y_j} = H_{\mathrm{Initial}}\left(x_i,\ y_j\right) \tag{5}$$

where n and m are the dimensions of the dwell-point matrix and are related to the step length (d) of the dwell-point grid.

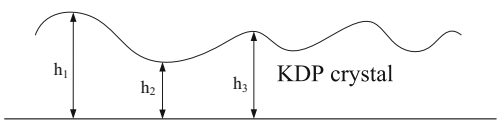

Fig. 9 Schematic diagram of the surface profile of a KDP crystal that shows the initial heights of the asperities, as measured with an interferometer

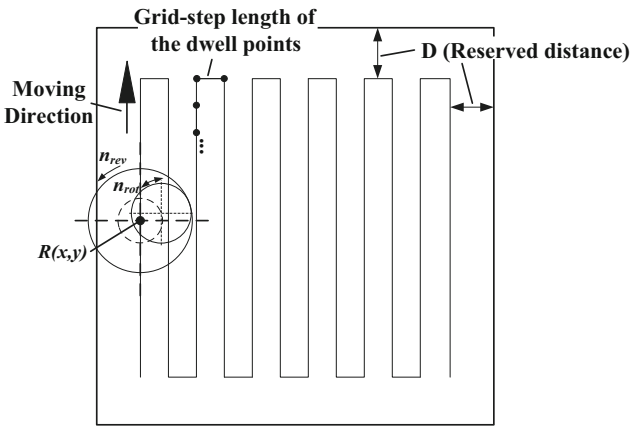

Fig. 10 Schematic diagram of the polishing path

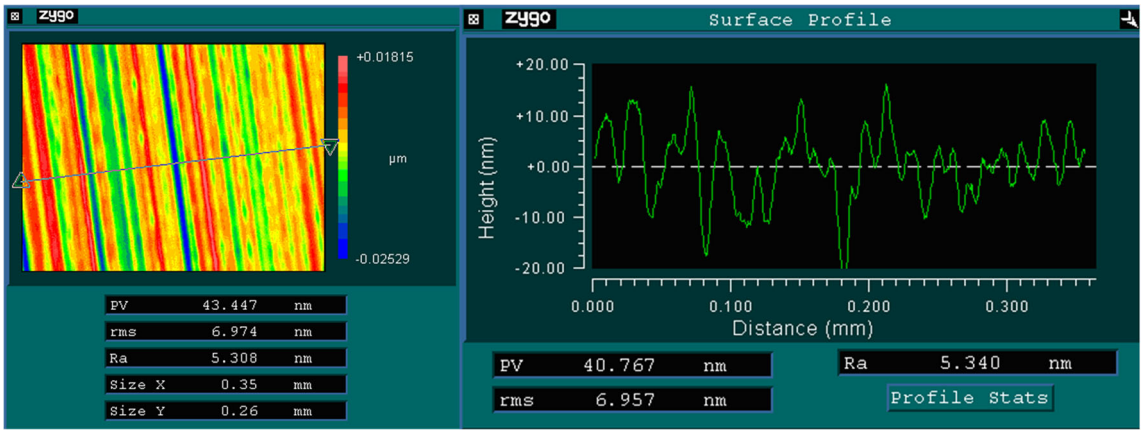

Fig. 11 Micro-waviness of the SPDT-machined KDP crystal

The value of n can be adjusted during the actual polishing process depending on the quality and size of the KDP crystal, e.g., during an ultra-precision polishing process, d is decreased (the density of dwell points on the grid density is increased). According to Eq. (5), the dwell-time distribution is determined by solving Eq. (5) for the polishing process of the KDP crystal.

The surface is then measured after the polishing process. If the accuracy of the polished surface is not satisfactory, the above process is then iterated until the surface accuracy meets the required level.

2.4 Measuring the initial surface topography of the KDP sample

The size of the KDP crystal after the SPDT process, but before the polishing process, was 50×50×10 mm. The micro-waviness of the SPDT-machined KDP crystal was measured with a three-dimensional profilometer (ZYGO Newview 5022) over an area of 0.35×0.26 mm. Figure 11 shows that the amplitude of the micro-waviness ranges from 20 to 30 nm and has a period of approximately 25 µm. The surface interferogram of the SPDT-machined KDP crystal was measured with an interferometer (Flatmaster 200), as shown in Fig. 12, to determine the amount of material to remove. The SPDT-machined KDP crystal exhibits a high surface accuracy (PV value of 0.498λ).

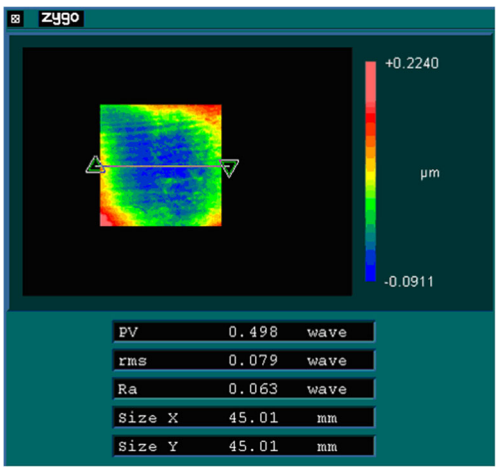

Fig. 12 Surface interferogram of the SPDT-machined KDP crystal (valid dimensions=90 % of the central region)

Tie et al. [13] measured the depth of the damaged subsurface layer under various SPDT parameters (e.g., feed rate, cutting depth, and cutting velocity) with the MRF spot method. In brief, a spot was polished at a particular location of the KDP crystal with the MRF method to expose the subsurface layer. The damaged subsurface layer was then observed along the axis of symmetry of the MRF-polished spot. The depth of the damaged subsurface layer was calculated with the geometric relationship between the profile of the MRF-polished spot and the position where there was no subsurface damage. The depth of the damaged subsurface layer as a function of the process parameters was reported. Thus, for the SPDT-machined KDP sample shown in Fig. 11, a depth of 200–300 nm was estimated according to the cutting parameters.

In general, a polishing method is widely used to measure the depth of the damaged subsurface layer because it is believed that the polishing method does not introduce any extra subsurface damage [23–26]. Moreover, a polishing process that uses the principles of water dissolution will further reduce the possibility of defects compared to traditional polishing methods. In this study, it is believed that there is no subsurface damage in the KDP crystal after it is adequately polished.

2.5 Determining the experimental removal function

To uniformly remove the micro-waviness and damaged subsurface layer while improving the surface accuracy, a

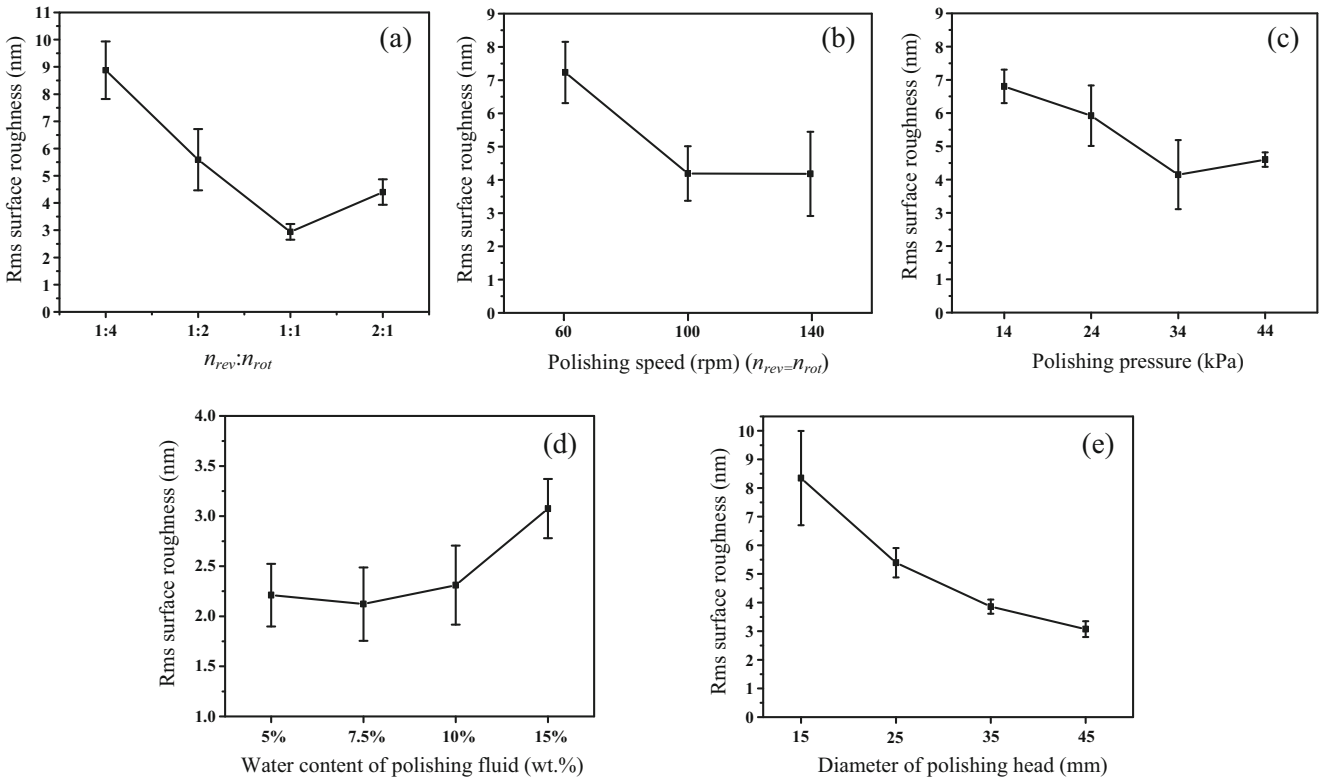

Fig. 13 Effects of the polishing parameters on the surface roughness of KDP crystals. **a** Ratio of n_{rev} to n_{rot} of the planetary motion of the polishing tool. **b** Polishing speed when n_{rev}:n_{rot}=1:1. **c** Polishing pressure. **d** Water content of the polishing fluid. **e** Diameter of the polishing head. [27]

suitable removal function must be chosen to determine the dwell time of the polishing process. The polishing head executes a planetary motion, and a Rohm & Hass IC1000 single-layer polyurethane pad was used in this study. The polishing parameters (e.g., the ratio of n_{rev} to n_{rot}, polishing speed, polishing pressure, diameter of the polishing tool, and water content of the polishing fluid) must be optimized to achieve a low surface roughness, and the effect of the polishing parameters on the surface roughness of KDP crystals has been investigated in the previous study by the authors of this paper [27] (as shown in Fig. 13).

To establish the experimental material removal function, an experiment was conducted on a KDP crystal. Before polishing the sample, the initial surface topography was measured with an interferometer to act as a reference plane. The polishing head then executed planetary motion with its center remaining immobile. Due to

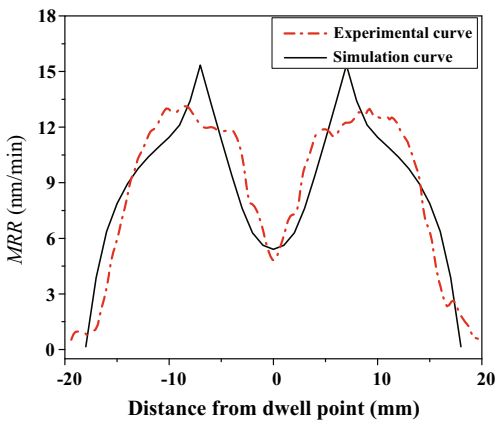

Fig. 14 Simulated and experimental curves of the MRR

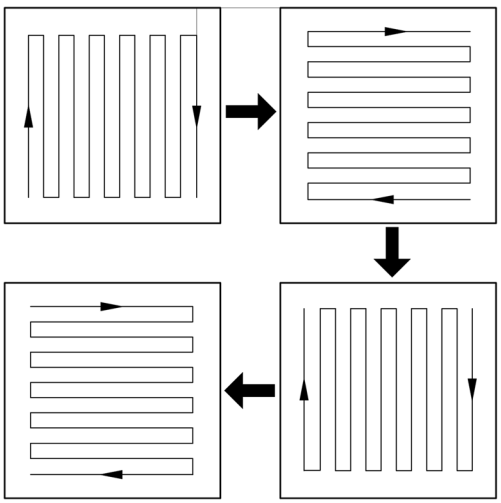

Fig. 15 Schematic diagram of the polishing paths applied to the KDP sample to remove the micro-waviness

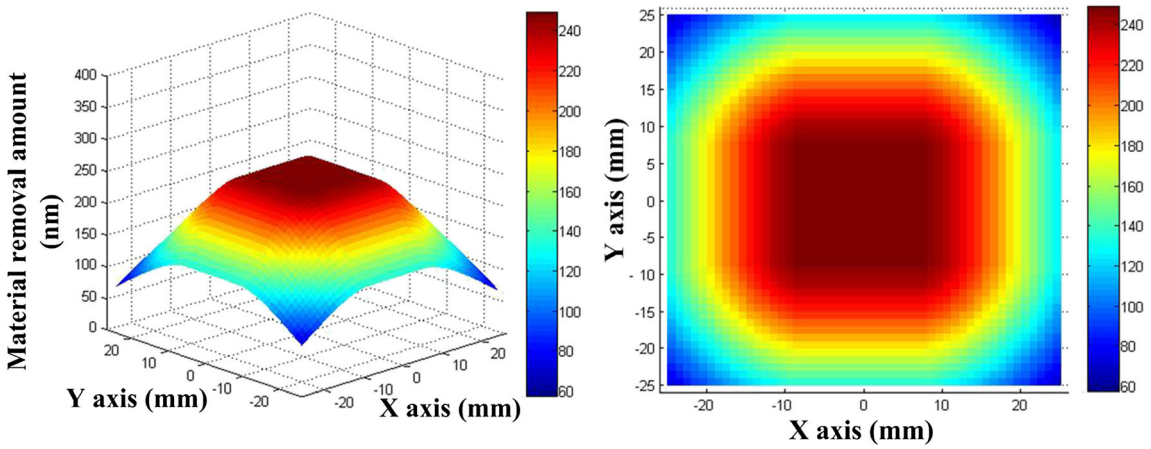

Fig. 16 Simulation of the material removal distribution (units of elevation=nm)

the micro dimension of waviness on initial surface, the material removal rate needs to be controlled at an appropriate level. In order to improve surface quality while reducing the material removal rate, the polishing parameters were selected according to the plots shown in Fig. 13. Because of the dimensions of the SPDT-machined KDP sample (50×50 mm), a polishing head with a diameter of 25 mm was used in this study. The n_{rev} and n_{rot} were both set to 100 rpm, and the polishing pressure was 40 kPa. The eccentricity which has no obvious influence on surface roughness was 5 mm. The water content of the polishing fluid was 4–7 wt.%.

After polishing the sample for 30 min, the polished surface topography was measured with the interferometer and subtracted from that of the reference plane to obtain the experimental curve for the material removed (the dash-dot line in Fig. 14). Figure 14 shows that the experimental curve is in good agreement with the simulated results, which proves the accuracy of the model used for the material removal function.

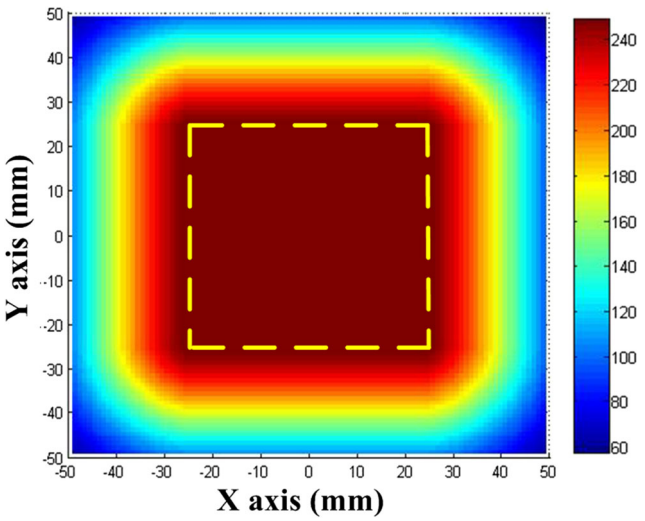

Fig. 17 Simulation of the material removal distribution when polishing with the protective blocks (units of elevation=nm)

2.6 Planning the polishing path

The uniform polishing raster path shown in Fig. 15 was chosen to process the KDP crystals after the SPDT machining because of the high surface accuracy after the SPDT process, which has met the needs of this study (KDP crystals used in practical engineering applications could achieve higher surface accuracies via SPDT machining). The center-of-revolution performs a reciprocating motion in the vertical direction at a constant speed until the whole surface is covered. The direction of the reciprocating motion is then changed from the vertical direction to the horizontal direction to eliminate any machining marks caused by the polishing tool. After three changes in the reciprocating direction, the polishing head returns to the starting point of the polishing path. Thus, the uniform polishing of a KDP crystal is achieved by repeatedly changing the polishing feed direction.

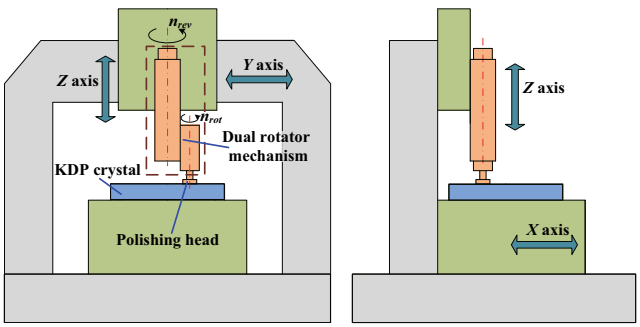

Fig. 18 Schematic diagram of the polishing equipment

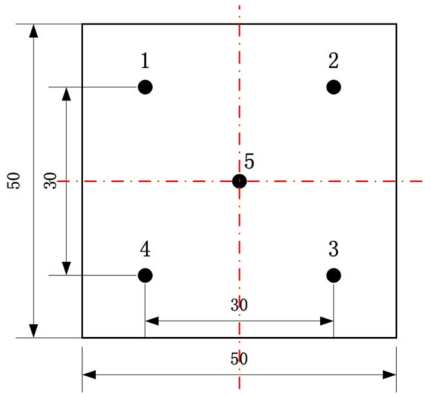

Fig. 19 Schematic diagram showing the five measurement points on the KDP crystal (units=mm)

When a uniform path is adopted for the polishing process, i.e., the dwell time at each dwell point on the crystal surface is equal, the dwell-time function in Eq. (5) is reduced to a constant (T). In view of this, $H_{\text{removal}}(x, y)$ is transformed into Eq. (6).

$$H_{\text{removal}}\left(x_i,\ y_j\right) = T\sum_{i=1,j=1}^{i=n,j=m} \text{MRR}_{x_i y_j}\left(r_i,\ \theta_j\right) \tag{6}$$

In the polishing experiments, the grid step length of the dwell points was 3 mm, and D was 8 mm to account for the size of the polishing head. According to the estimated depth of the damaged subsurface layer, $H_{\text{removal}}(x, y)$ was set to 250 nm to remove all traces of the micro-waviness and subsurface damage. By substituting 250 nm into Eq. (6), a dwell time of T=0.23 min was obtained for each point, and $H_{\max}$= 248.6 nm was obtained by using T=0.23 min in Eq. (6) (Fig. 16).

Based on the polishing path shown in Fig. 15, the polishing tool scans each dwell point four times during a single iteration of the polishing process. Therefore, the expression for the dwell time can be written as follows:

$$T = 4(d/F)N \tag{7}$$

where d is the length of the grid step (3 mm), F is the feed speed of the revolving center of the polishing head, and N is the number of iterations.

To ensure the uniformity of the polishing process, the number of iterations is increased to reduce the dwell time at each point in the polishing process. In this study, the number of iterations was 6 (N=6). The polishing feed speed can be solved by substituting N= 6 into Eq. (7), resulting in F=313 mm/min, which was rounded down to F=300 mm/min.

The amount of material removed from the edges of the crystal surface is less than that in the central area because of D, and the shape of the polishing removal distribution is a square frustum (Fig. 16). The material removal distribution in the central polishing area of the crystal surface is uniform, and this planar region of the material removal distribution is dependent upon the size of the polishing tool and D. To improve the quality of the polished surface, the size of this uniform plane must be enlarged.

Decreasing the size of the polishing head also decreases the size of D and increases the size of the uniform plane. However, a reserved distance still exists because the polishing head cannot completely move off the crystal surface with this method. In this study, protective blocks were arranged around the KDP crystal with the purpose of enlarging the size of the uniform plane. Four rectangular KDP crystals with appropriate sizes were ground to the same height, which was equal to the height of the SPDT-machined KDP crystal, and closely placed around the crystal. The KDP crystal and the four protective blocks were fixed in place with a vacuum chuck. Therefore, the polishing head was able to move to the edges of the KDP crystal surface without tilting, and the region that is divided into the grid was expanded to enlarge the central polishing area.

Based on these theoretical calculations, the uniform plane was increased to cover the entire KDP crystal surface by increasing the dimensions of the dwell-point grid to 84×84 mm. Figure 17 shows that the coordinate values range from −25 to +25 mm (the area indicated by the dashed yellow line), which is the KDP crystal surface.

3 Experimental study

3.1 Experimental conditions

An experimental study to remove the SPDT-induced micro-waviness was performed to verify the feasibility of the new method with a homemade, five-axis, optical polishing setup (Fig. 18). The polishing experiments were conducted in a clean room (class 1000) at 25 °C under a relative humidity of 50 %. The optimized polishing parameters and polishing path described in Section 2 were used.

To ensure that the measurements of the micro-waviness and surface roughness were accurate, five points on the KDP crystal were measured with the three-dimensional profilometer, as shown in Fig. 19, and the results of the five measurements were averaged.

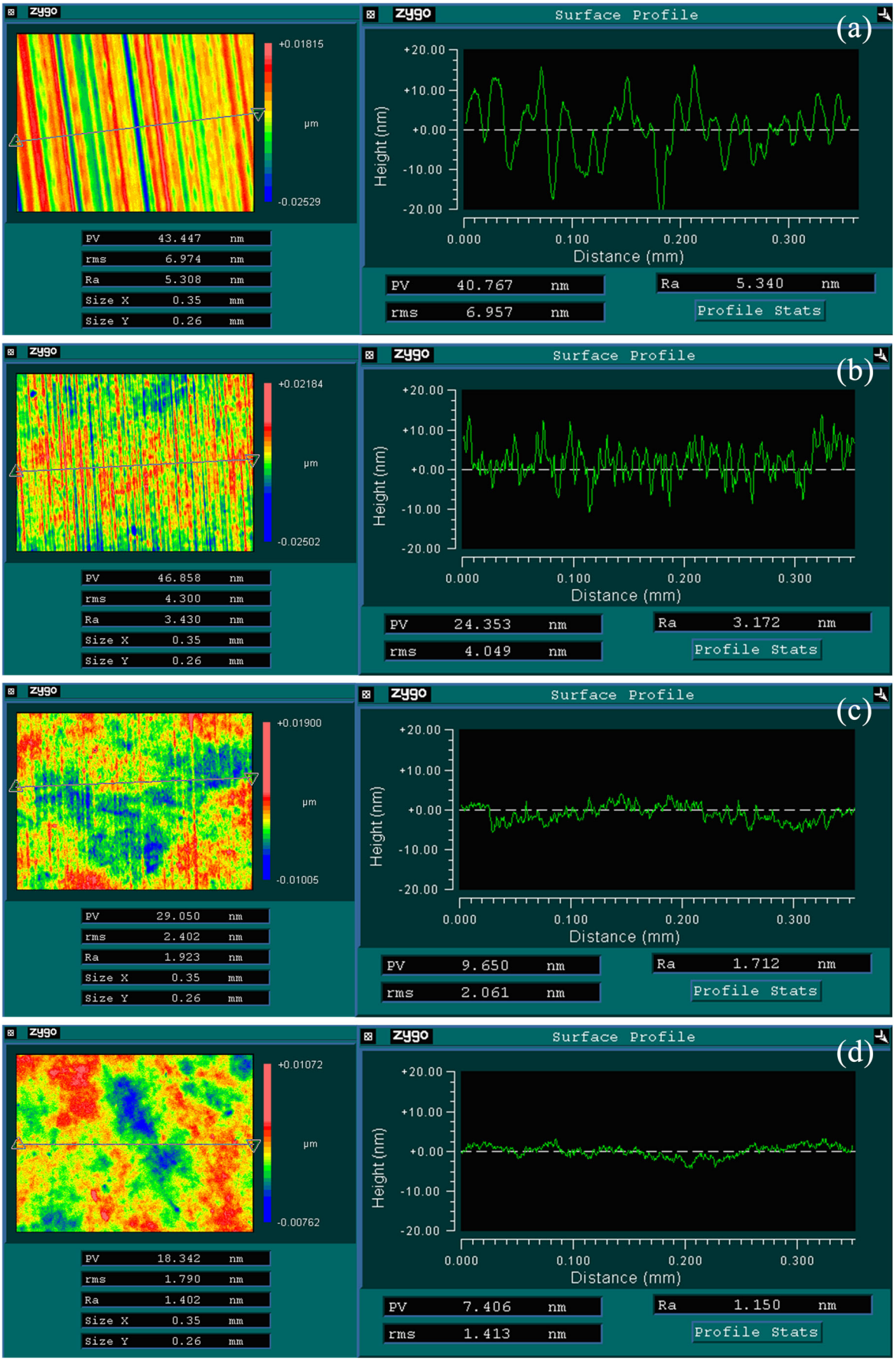
zygo
+0.01815
µm
-0.02529
PV 43.447 nm
rms 6.974 nm
Ra 5.308 nm
Size X 0.35 mm
Size Y 0.26 mm
zygo
Surface Profile
(a)
+20.00
+10.00
+0.00
-10.00
-20.00
Height (nm)
0.000
0.100
0.200
0.300
Distance (mm)
PV 40.767 nm
rms 6.957 nm
Ra 5.340 nm
Profile Stats
zygo
+0.02184
µm
-0.02502
PV 46.858 nm
rms 4.300 nm
Ra 3.430 nm
Size X 0.35 mm
Size Y 0.26 mm
zygo
Surface Profile
(b)
+20.00
+10.00
+0.00
-10.00
-20.00
Height (nm)
0.000
0.100
0.200
0.300
Distance (mm)
PV 24.353 nm
rms 4.049 nm
Ra 3.172 nm
Profile Stats
zygo
+0.01900
µm
-0.01005
PV 29.050 nm
rms 2.402 nm
Ra 1.923 nm
Size X 0.35 mm
Size Y 0.26 mm
zygo
Surface Profile
(c)
+20.00
+10.00
+0.00
-10.00
-20.00
Height (nm)
0.000
0.100
0.200
0.300
Distance (mm)
PV 9.650 nm
rms 2.061 nm
Ra 1.712 nm
Profile Stats
zygo
+0.01072
µm
-0.00762
PV 18.342 nm
rms 1.790 nm
Ra 1.402 nm
Size X 0.35 mm
Size Y 0.26 mm
zygo
Surface Profile
(d)
+20.00
+10.00
+0.00
-10.00
-20.00
Height (nm)
0.000
0.100
0.200
0.300
Distance (mm)
PV 7.406 nm
rms 1.413 nm
Ra 1.150 nm
Profile Stats

◀ **Fig. 20** Surface topography of the KDP crystal after various polishing iterations (the center of the KDP surface, point no. 5 in Fig. 19). **a** Crystal surface after the SPDT machining process (before being polished). **b–d** Crystal surface after 2 (**b**), 4 (**c**), and 6 (**d**) polishing iterations

3.2 Experimental results and discussion

The surface topography of the KDP sample before the polishing process is shown in Fig. 20a (the same as the sample shown in Fig. 11). The average rms surface roughness is 6.206 nm, while the average profile surface roughness (R_a) is 4.822 nm. The micro-waviness is obvious, and its amplitude ranges from 20 to 30 nm.

During the polishing process, the surface roughness changed with the number of polishing iterations, as shown in Fig. 21. The surface roughness of the sample rapidly reduces at the beginning of the polishing process, and then, the rate of change becomes relatively gentle. After two polishing iterations, the micro-waviness is still present, but its amplitude has been greatly reduced (Fig. 20b). After four polishing iterations, the surface roughness and micro-waviness of the KDP crystal have been significantly reduced, with only the deepest cutting marks still present on the surface (Fig. 20c). Figure 20d shows the surface topography after six polishing iterations. In this case, the undulation of the surface has been significantly decreased to 8–10 nm and the initial micro-waviness has been completely removed.

In addition, after the polishing process, the average rms surface roughness of the KDP sample has been reduced to 2.107 nm, while the average R_a value has decreased to 1.674 nm. Compared to the initial surface figure (0.498λ PV, Fig. 12), the surface figure has been improved slightly (0.308λ PV, Fig. 22).

Atomic force microscopy (AFM, XE-200, Park Systems) was used to observe the crystal surface before and after the polishing process (measuring area=10×10 μm). By comparing the high-resolution mapping results of the initial (Fig. 23a) and polished (Fig. 23b) surfaces, the SPDT-induced micro-waviness has been completely removed by the micro-dissolution polishing method, and the surface after the polishing process is nearly a super-smooth plane. Figure 24 shows the power spectral density (PSD) curves of the KDP surface before and after the polishing process, which demonstrates that the surface errors have been improved. The absence of peaks that range in size from 15.9 to 49.3 mm^{-1}, which are caused by the SPDT machining, proves that the surface quality is improved by the micro-dissolution polishing method.

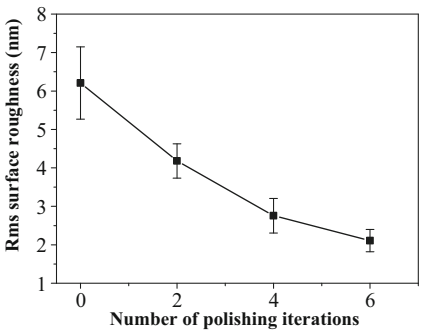

Fig. 21 Variation of the rms surface roughness of the KDP crystal as a function of the number of polishing iterations

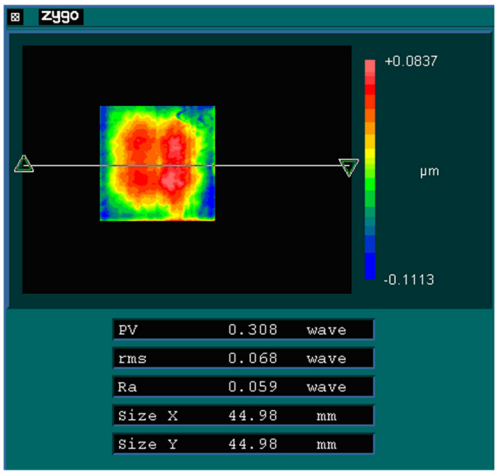

Fig. 22 Surface interferogram of the KDP crystal after completing the polishing process (valid dimensions=90 % of the central region)

To evaluate the effects of the water-dissolution polishing on the laser-damage performance versus that obtained with SPDT machining, a 1-on-1 laser-damage test was performed on KDP samples. A Nd:YAG laser (355 nm, pulse duration= 6.8 ns) was used for the tests, and the laser beam area was 0.22 mm^2. Figure 25 shows the damage probability of the KDP crystal after the water-dissolution polishing and SPDT machining as a function of the laser energy density. The plots have been fitted with a linear function to obtain the laser-induced damage threshold by extending the fits to the damage probability of zero. The laser-induced damage threshold of the sample obtained with water-dissolution polishing is 3.21 J/cm^2, which is higher than that obtained after the SPDT machining (2.30 J/cm^2).

According to the results of the preliminary laser-damage test, the water-dissolution polishing method improves the laser-induced damage threshold of the SPDT-machined KDP crystal. In addition, the results of further laser-damage tests for more sample processing methods and other types of laser (λ= 1064 and 532 nm) will be reported in a future paper.

4 Conclusions

By incorporating the principles of micro-dissolution water polishing into a computer-controlled optical surfacing technique, a new polishing method was developed

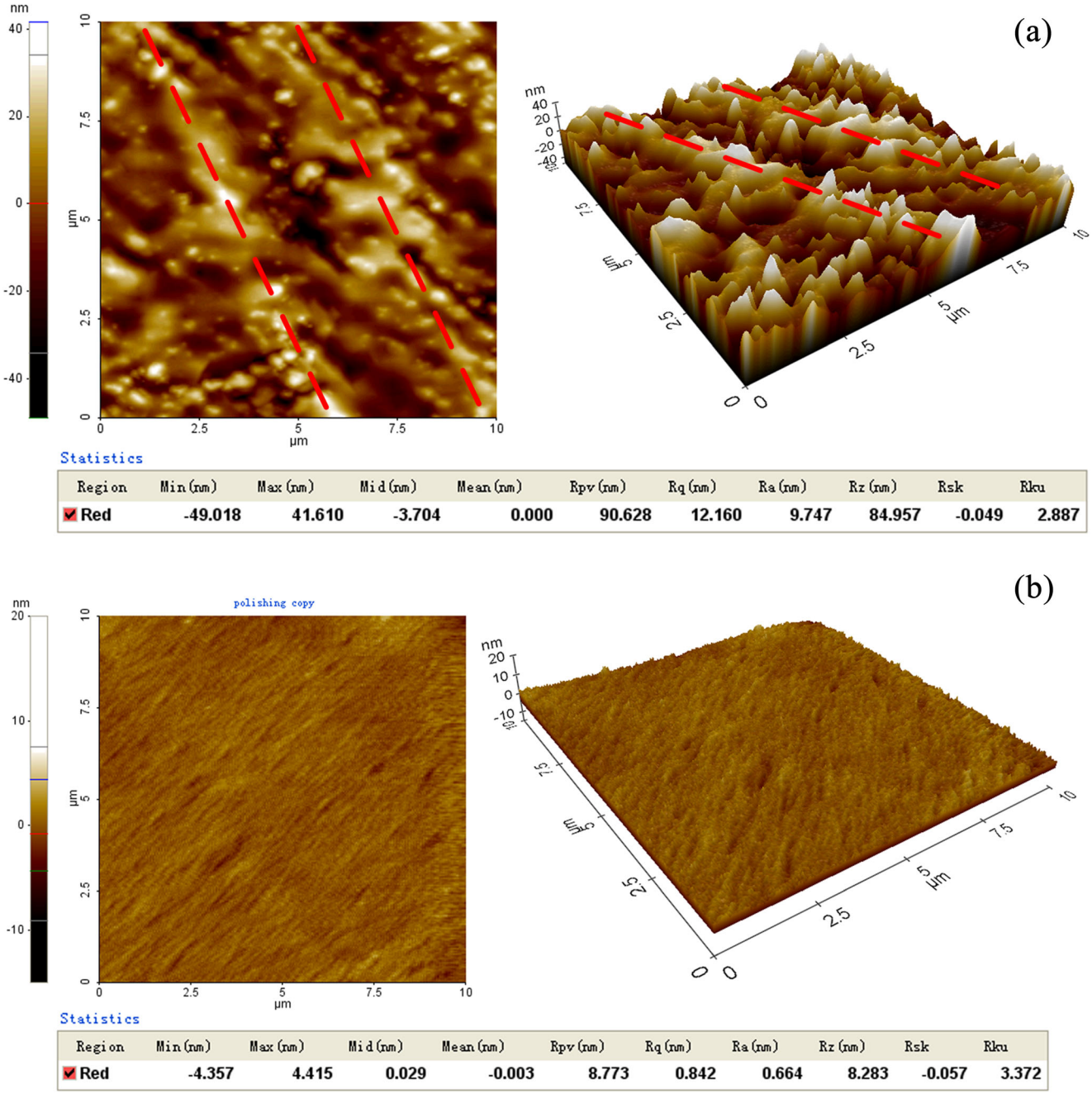

Fig. 23 AFM measurements of the KDP surface **a** before and **b** after the polishing process. The *dashed lines* in (**a**) indicate the locations of the maximum micro-waviness

that uses a W/O-structured micro-emulsion as the polishing fluid for KDP crystals to remove the micro-waviness of the SPDT-machined surface. The following conclusions were obtained.

(1) Based on the principles of micro-dissolution polishing, a material removal function was established and verified with an experimental investigation.

(2) The optimum removal function, which was obtained by optimizing the polishing parameters was adopted in this study to remove the micro-waviness. The optimum polishing path was derived according to the initial topography of the KDP surface.

(3) After the polishing process, the micro-waviness of the SPDT-machined surface was completely removed and the surface quality was improved (rms and R_a surface

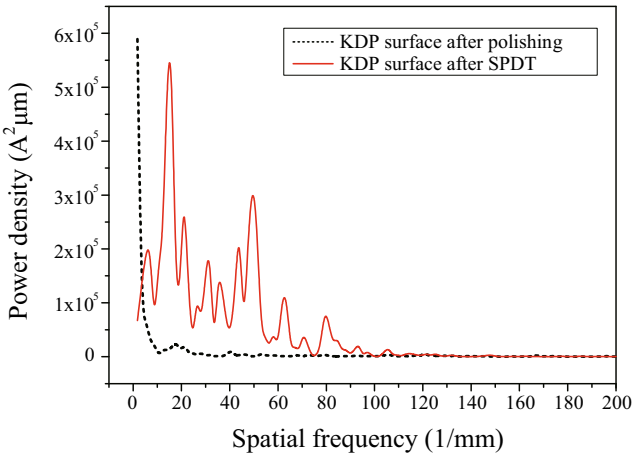

Fig. 24 PSD analysis

roughnesses were reduced from 6.205 and 4.822 nm to 2.107 and 1.674 nm, respectively; the surface-figure error was reduced from 0.498λ PV to 0.308λ PV). The enhanced smoothness of the surface after the polishing process was confirmed with PSD analysis.

(4) According to the results of the preliminary laser-damage tests (355 nm, pulse duration=6.8 ns), the water-dissolution polishing method improved the laser-induced damage threshold of the SPDT-machined KDP crystal. The laser-induced damage threshold of the sample obtained with water-dissolution polishing was 3.21 J/cm^2, which was higher than that of the SPDT-machined surface (2.30 J/cm^2).

To improve both the polishing efficiency and surface quality after the polishing process, the dwell time and polishing path must be optimized. Further research on such subjects is required, and the results will be reported in a future paper. This novel method for micro-dissolution polishing provides a new approach for achieving the ultra-precision machining of water-soluble materials.

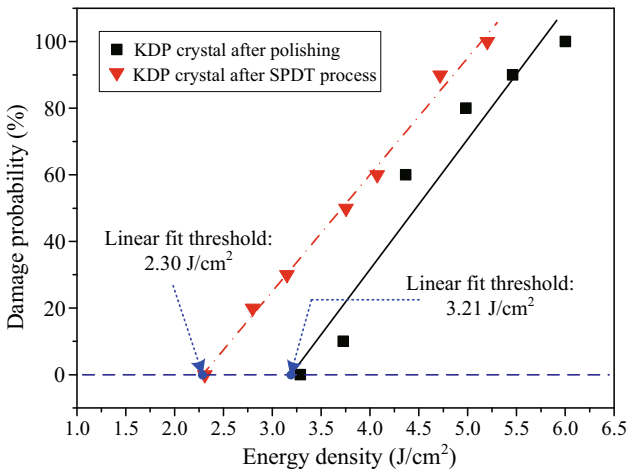

Fig. 25 Laser-induced damage threshold of the KDP crystal after the water-dissolution polishing and SPDT machining

Acknowledgments This work was funded by the National Natural Science Foundation of China (Grant No. 51135002) and Science Fund for Creative Research Groups (Grant No. 51321004).

References

1. Moses EI (2010) Advances in inertial confinement fusion at the National Ignition Facility (NIF). Fusion Eng Des 85(7):983–986
2. Campbell JH, Hawley-Fedder RA, Stolz CJ, Menapace JA, Borden MR, Whitman PK, Yu J, Runkel M, Riley MO, Feit MD, Hackel RP (2004) NIF optical materials and fabrication technologies: an overview. Proc SPIE 5341:84–101
3. Hurricane OA, Callahan DA, Casey DT, Celliers PM, Cerjan C, Dewald EL, Dittrich TR, Doppner T, Hinkel DE, Hopkins LF, Kline JL, LePape S, Ma T, MacPhee AG, Milovich JL, Pak A, Park HS, Patel PK, Remington BA, Salmonson JD, Springer PT, Tommasini R (2014) Fuel gain exceeding unity in an inertially confined fusion implosion. Nature 506(7488):343–349
4. Yoshiharu N, Masanori K (1999) Ultraprecision grinding of potassium dihydrogen phosphate crystals for getting optical surfaces. Proc SPIE 3578:692–693
5. Peng XQ, Jiao FF, Chen HF, Tie GP, Shi F, Hu H (2011) Novel magnetorheological figuring of KDP crystal. Chin Opt Lett 9(10): 102201
6. Arrasmith SR, Kozhinova IA, Gregg LL, Shorey AB, Romanofsky HJ, Jacobs SD, Golini D, Kordonski WI, Hogan S, Dumas P (1999) Details of the polishing spot in magnetorheological finishing (MRF). Proc SPIE 3782:92–100
7. Wang B, Wu DJ, Gao H, Kang RK (2009) Influence of cleaning method on quality of KDP crystal polished surface. J Synth Cryst 38(2):525–528
8. Hou J, Zhang JF, Chen JL, Zhang XL, Hu DZ (2006) Surface quality of large KDP crystal fabricated by single-point diamond turning. Proc SPIE 6149:1–3
9. Chen MJ, Pang QL, Wang JH, Chen K (2008) Analysis of 3D micro topography in machined KDP crystal surfaces based on fractal and wavelet methods. Int J Mach Tools Manuf 489(7):905–913
10. Chen MJ, Li MQ, Jiang W, Xu Q (2010) Influence of period and amplitude of microwaviness on KH_2PO_4 crystal's laser damage threshold. J Appl Phys 108(4):43109
11. Chen WQ, Lu LH, Yang K, Huo DH, Su H, Zhang QC (2015) A novel machine tool design approach based on surface generation simulation and its implementation on a fly cutting machine tool. Int J Adv Manuf Technol 80(5):829–837
12. Liang YC, Chen WQ, Bai QS, Sun YZ, Chen GD, Zhang Q, Sun Y (2013) Design and dynamic optimization of an ultraprecision diamond flycutting machine tool for large KDP crystal machining. Int J Adv Manuf Technol 69(1–4):237–244
13. Tie GP, Dai YF, Guan CL, Chen SS, Song B (2013) Research on subsurface defects of potassium dihydrogen phosphate crystals fabricated by single point diamond turning technique. Opt Eng 52(3): 33401
14. Jacobs SD (2007) Manipulating mechanics and chemistry in precision optics finishing. Sci Technol Adv Mater 8(3):153–157
15. Menapace JA, Ehrmann PR, Bickel RC (2009) Magnetorheological finishing (MRF) of potassium dihydrogen phosphate (KDP)

crystals: nonaqueous fluids development, optical finish, and laser damage performance at 1064 nm and 532 nm. Proc SPIE 7504:1–14
16. Zhang FH, Guo SL, Zhang Y, Luan DR (2009) Research on the material removal mechanism in deliquescent polishing of KDP crystals. Key Eng Mater 416:487–491
17. Wang BL, Li YZ, Gao H (2010) Water-in-oil dispersion for KH_2PO_4 (KDP) crystal CMP. J Dispers Sci Technol 31(12):1611–1617
18. Zhang HP, Guo DM, Wang X, Gao H (2012) Simulation of large scale KDP crystal polishing by computer controlled micro-nano deliquescence. Adv Mater Res 497:165–169
19. Gao H, Wang BL, Guo DM, Li YZ (2010) Experimental study on abrasive-free polishing for KDP crystal. J Electrochem Soc 157(9):853–856
20. Wang BL (2010) Abrasive-Free water-dissolution polishing and processing mechanism for KDP crystal. Dissertation, Dalian University of Technology
21. Wang C, Yang W, Ye S, Wang ZZ, Yang P, Peng Y, Guo Y, Xu Q (2014) Restraint of tool path ripple based on the optimization of tool step size for sub-aperture deterministic polishing. Int J Adv Manuf Technol 75(9–12):1431–1438
22. Li L, Zheng L, Deng W, Wang X, Wang XK, Zhang BZ, Bai Y, Hu HX, Zhang XJ (2015) Optimized dwell time algorithm in magnetorheological finishing. Int J Adv Manuf Technol. doi:10.1007/s00170-015-7263-3
23. Wang B, Wu DJ, Gao H, Kang RK, Guo DM (2009) Subsurface damage in scratch testing of potassium dihydrogen phosphate crystal. Chin J Mech Eng 22(1):15–20
24. Lv DX, Huang YH, Tang YJ, Wang HX (2013) Relationship between subsurface damage and surface roughness of glass BK7 in rotary ultrasonic machining and conventional grinding processes. Int J Adv Manuf Technol 67(1–4):613–622
25. Wang CC, Fang QH, Chen JB, Liu YW, Jin T (2015) Subsurface damage in high-speed grinding of brittle materials considering kinematic characteristics of the grinding process. Int J Adv Manuf Technol. doi:10.1007/s00170-015-7627-8
26. Wang J, Zhang CL, Feng PF, Zhang JF (2015) A model for prediction of subsurface damage in rotary ultrasonic face milling of optical K9 glass. Int J Adv Manuf Technol. doi:10.1007/s00170-015-7567-3
27. Wang X, Gao H, Chen YC, Teng XJ (2015) The impact of micro water dissolution polishing parameters on the surface roughness of KDP crystal. J Synth Cryst 44(10):2702–2707